DRL-58-DRD-SE 7

DOE/JPL 954373-79/11
Distribution Category UC-63

SILICON INGOT CASTING - HEAT EXCHANGER METHOD MULTI-WIRE SLICING- FIXED ABRASIVE SLICING TECHNIQUE

Phase III

Silicon Sheet Growth Development for the
Large Area Sheet Task of the Low-Cost Solar Array Project

QUARTERLY PROGRESS REPORT NO. 3

BY

FREDERICK SCHMID AND CHANDRA P. KHATTAK

Covering Period from April 1 through June 30, 1979
Report Issued: July 1979
JPL Contract No. 954373

CRYSTAL SYSTEMS INC.
Shetland Industrial Park, 35 Congress Street, Salem, Mass. 01970

DRL-58-DRD-SE 7

DOE/JPL 954373 - 79/11
Distribution Category U-63

SILICON INGOT CASTING - HEAT EXCHANGER METHOD

MULTI-WIRE SLICING - FIXED ABRASIVE SLICING TECHNIQUE

(PHASE III)

Silicon Sheet Growth Development for the
Large Area Sheet Task of the
Low-Cost Solar Array Project

Quarterly Progress Report No. 3

by

Frederick Schmid and Chandra P. Khattak

Covering Period from April 1 through June 30, 1979

Report Issued: July 1979

JPL Contract No. 954373

CRYSTAL SYSTEMS, INC.
35 Congress Street
Salem, MA 01970

The JPL Low-Cost Solar Array Project is sponsored by the U. S. Department of Energy and forms part of the Solar Photovoltaic Conversion Program to initiate a major effort toward the development of low-cost solar arrays. This work was performed for the Jet Propulsion Laboratory, California Institute of Technology by agreement between NASA and DOE.

This report contains information prepared by Crystal Systems, Inc., under JPL subcontract. Its content is not necessarily endorsed by the Jet Propulsion Laboratory, California Institute of Technology, National Aeronautics and Space Administration or the U. S. Department of Energy.

TABLE OF CONTENTS

	Page
TABLE OF CONTENTS	iii
ACKNOWLEDGMENT	iv
ABSTRACT	v
SILICON INGOT CASTING--HEAT EXCHANGER METHOD	1
Ingot Casting	1
Crucible Development	10
MULTI-WIRE SLICING--FIXED ABRASIVE SLICING TECHNIQUE	11
Machine Development	11
Blade Development	17
CONCLUSIONS	21
REFERENCES	22
MILESTONE CHART	23
APPENDIX	25

ACKNOWLEDGEMENT

The authors wish to acknowledge the valuable assistance and contributions from John A. Lesiczka, Barbara B. Nelson, and Maynard B. Smith.

ABSTRACT

Ingot casting has been scaled up to 16 cm x 16 cm square cross-section size weighing up to 8.1 kg. The high degree of crystallinity has been maintained in the large ingot. For large sizes, the non-uniformity of heat treatment causes "chipping" of the surface of the ingot. Significant effort and progress has been made in the development of a uniform graded structure in the silica crucibles.

The high speed slicer has been modified so that the blade-head weight is reduced to 37 pounds. This has allowed higher surface speeds of up to 500 feet per minute. Slicing of 10 cm diameter workpieces at these speeds has increased the through-put of the machine to 5.7 mils/min., 0.145 mm/min., 50 per cent more than the projected cutting rates used in the economic analysis.

SILICON INGOT CASTING -- HEAT EXCHANGER METHOD

The emphasis in silicon casting during the current quarter has been on improvement of the solidification cycle, crucible development and scale-up. Significant advances have been made and ingots up to 8.1 kg weight in 16 cm x 16 cm square cross-section have been cast.

Ingot Casting

It is intended to cast large silicon ingots by the Heat Exchanger Method (HEM). It has been found[1] that the melt temperature during crystal growth has to be maintained very close to the melting point of silicon. This is associated with the higher conductivity of silicon in the liquid state as compared to the solid state. Under such conditions growth is impeded since heat is transferred rapidly from the crucible wall to the solid-liquid interface via the molten silicon. It is, therefore, necessary to keep the temperature of the melt as close to the melt point as the instrumentation will allow. In the HEM the submerged interface and uniform temperature gradients at the solid-liquid interface prevent spurious nucleation even at such low superheat.

Another feature observed during crystal growth of silicon by HEM was an increase in power levels as the solidification progressed. This was particularly noticeable towards the end of the growth cycle. The growth cycle was initiated by increasing the flow of helium gas through the heat exchanger. Solidification proceeded and the heat exchanger reduced the temperature of the melt. The furnace controller compensated for the heat extraction by increasing power to the heater to maintain a constant furnace temperature. When the size of ingot grown was small compared to the size of the heat zone, this effect was not very large. However, for large ingots, these mutually compensating effects of heat extraction by heat exchanger and increase in power to the furnace have to be minimized. During runs 317-C through 322-C (details in Table I) the furnace was controlled on the basis of power rather than temperature. The sensitivity of control on power is not as accurate as with temperature. Under power control constant power is maintained; therefore, the furnace temperature decreased during the run due to the cooling effect of the heat exchanger. While controlling with power the melt temperature is slightly higher; hence, a period of stabilization takes place before any growth occurs. This increases the growth time. This period will be the same for larger ingots; hence growth rates will improve with size of the ingots cast. Additionally power control was reproducible from experiment to experiment. In earlier runs when deposits formed on the windows of the furnace, it led to incorrect

TABLE I. TABULATION OF HEAT-EXCHANGER AND FURNACE TEMPERATURES

RUN	PURPOSE	SEEDING		GROWTH CYCLE			REMARKS
		FURN. TEMP. ABOVE M.P. °C	H.E. TEMP. BELOW M.P. °C	RATE OF DECREASE H.E. TEMP. °C/HR.	RATE OF DECREASE FURN. TEMP. °C	GROWTH TIME IN HOURS	
317-C	Improve solidification cycle	8	160	161	8	6.5	Controlling with power
318-C	Improve solidification cycle	< 3	110	234	0	6.8	Controlling with power
319-C	Improve solidification cycle	3	100	256	3	5.5	Controlling with power
320-C(3)	Improve solidification cycle	3	152	226	3	6.3	Controlling with power
321-C	Improve solidification cycle	5	135	262	5	6.0	Controlling with power
322-C	Improve solidification cycle	< 3	165	258	0	4.8	Controlling with power
323-C	Improve uniformity of graded structure of crucible	< 3	213	237	2	4.5	Good crystallinity but attachment of crucible to ingot
324-C	Improve uniformity of graded structure of crucible	< 3	145	333	2	4.5	Crucible attached to ingot

(cont.)

TABLE I. TABULATION OF HEAT-EXCHANGER AND FURNACE TEMPERATURES (cont.)

RUN	PURPOSE	SEEDING		GROWTH CYCLE			REMARKS
		FURN. TEMP. ABOVE M.P. °C	H.E. TEMP. BELOW M.P. °C	RATE OF DECREASE H.E. TEMP. °C/HR.	RATE OF DECREASE FURN. TEMP. °C	GROWTH TIME IN HOURS	
325-C	Crucible development using lathe	< 3	145	416	0	4.5	Crucible attachment caused cracking
326-C	Crucible development using lathe	< 3	163	295	0	5.7	Crucible attachment caused cracking
327-C	Crucible development using lathe	4	133	346	4	4.0	Good crystallinity achieved
328-C (4)	Crucible development using lathe	3	146	314	3	4.5	Good crystallinity achieved
329-C	Cast 4.5 kg, 16 cm x 16 cm square ingot	< 3	135	287	0	5.7	Crack-free ingot cast
330-C	Cast 16 cm x 16 cm square ingot	< 3	115	330	0	6.0	Minor attachment in bottom area
331-C	Cast 8.1 kg, 16 cm x 16 cm square ingot	4	110	360	4	14.5	Minor attachment in bottom area
332-C	Cast 4.3 kg, 16 cm x 16 cm square ingot	4	96	246	3	5.75	Very good crystallirity
333-C	Cast 4.3 kg, 16 cm x 16 cm square ingot	< 3	95	362	0	6.00	Very good crystallinity

(cont.)

TABLE I. TABULATION OF HEAT-EXCHANGER AND FURNACE TEMPERATURES (cont.)

RUN	PURPOSE	SEEDING		GROWTH CYCLE			REMARKS
				RATE OF DECREASE			
		FURN. TEMP. ABOVE M.P. °C	H.E. TEMP. BELOW M.P. °C	H.E. TEMP. °C/HR.	FURN. TEMP. °C	GROWTH TIME IN HOURS	
334-C	Cast 4.3 kg, 16 cm x 16 cm square ingot	4	93	274	4	6.5	Minor chipping of ingot
335-C	Cast 4.3 kg, 16 cm x 16 cm square ingot	15	109	308	15	6.75	Very good crystallinity
336-C	Cast 4.3 kg, 16 cm x 16 cm square ingot	-	-	-	-	-	Run terminated; reaction of Si with graphite pipe
337-C	Cast 8.2 kg ingot (S)	-	-	-	-	-	Run terminated; Heat Exchanger failure
338-C	Cast 7.7 kg ingot	11	205	400	11	16.5	Minor chipping of ingot

temperature measurement and thereby prolonged growth cycles.

Very good crystallinity of the silicon ingots has been maintained.

A major emphasis of the present program is to cast large, square cross-section ingots. During Phase II 10 cm x 10 cm ingots were cast. It was intended to scale up the size to 15 cm x 15 cm during the next step. The crucibles fabricated have an inside dimension which is close to about 17 cm x 17 cm. A 4.5 kg ingot cast in run 329-C is shown in Figure 1. This was the first ingot of this size that was cast.

During run 331-C the size of the ingot was almost doubled to 8.1 kg. No problems were encountered during crystal growth of this ingot. The as-cast surface of this ingot is shown in Figure 2. One of the major advantages of the Heat Exchanger Method (HEM) is its simplicity. This allows easy scale-up in size and this has been demonstrated again. However, the crystal growth from the bottom means that as the size is increased the interface is further away from the heat exchanger. So far the height to diameter/width of the ingot has always been slightly less than unity. In run 331-C the ingot cast was such that the height to width ratio was greater than one and no problems were encountered. A similar size ingot cast in run 338-C is shown in Figure 3.

Figure 1. Two views of the 16 cm x 16 cm square ingot cast by HEM in run 329-C.

Figure 2. A view of 8.1 kg square ingot as removed from crucible

Figure 3. A view of 8.1 kg square ingot cast in run 338-C

Crucible Development

In order to cast crack-free silicon ingots in silica crucibles it is necessary to develop a graded structure in the crucible. This structure has been developed by heat treatment manually and has worked satisfactorily. With larger crucible sizes it has been very difficult to achieve uniformity in the graded structure. A glass-working lathe has been procured. The crucibles are rotated at a constant rate and heated to develop a uniform graded structure. It is intended to mechanize this approach further to achieve a higher degree of uniformity. Once the conditions are standardized, it could be extended to still larger crucibles. Initially crucible development and optimization was conducted with 15 cm diameter crucibles. Once some experience was gained with the glass-working lathe for heat treatment of the 15 cm diameter crucibles, larger size 16 cm x 16 cm square crucibles were heat treated. The first such size was used in run 329-C and a 4.5 kg crack-free ingot was cast. During runs 330-C and 331-C minor attachment of the crucible to the bottom of the ingot was observed. This problem has since been corrected by heat treating the bottom area a little differently to correct for the different temperature of the bottom of the crucible as compared to the temperature profile of the sides of the crucible during crystal growth.

MULTI-WIRE SLICING--FIXED ABRASIVE SLICING TECHNIQUE

The emphasis during the current quarter in silicon slicing was on machine and blade development. Efforts were pursued to reduce the weight of the bladehead so that still higher speeds can be achieved.

Machine Development

It has been established[2] that for effective slicing with fixed diamond abrasive it is desirable to operate at high surface speeds. At lower speeds the diamond is in a dragging mode rather than in a cutting mode. In order to achieve higher speeds it is necessary to lighten the reciprocating bladehead. The weight of the modified Varian slicer was about 200 pounds and a surface speed of 100 feet per minute was achieved. The high speed slicer designed was such that the blade carriage was twice as long and weighed half as much. Slicing tests with this bladehead were carried out at surface speed of about 200 feet per minute.[2] Significant improvement of the cutting performance was seen at the higher speeds. To further increase speeds it was necessary to lighten the reciprocating carriage still further. A new 37 pound bladehead has been designed and

fabricated. A dry run test for speed has shown that 500 feet per minute surface speeds can be achieved. This lightweight blade carriage together with higher speeds is expected to show a big improvement in cutting performance.

One of the problems identified during slicing tests of 10 cm x 10 cm workpiece was the hysteresis of the feed mechanism and the shape of the cut profile. These problems have been solved by using weights to control feed forces and by altering the rocking mechanism so that a smooth cut profile is achieved.

Figure 4 shows two views of the new lightweight bladehead assembled in the slicer. Figure 5 shows the new rocking mechanism incorporated.

The first slicing test with the modified slicer was carried out during run 325-SX (details in Table II) to slice a 10 cm diameter silicon workpiece. The surface speed was about 400 feet per minute with a 16-inch stroke length. Very good cutting rates were achieved; such high cutting rates have never been achieved with commercially impregnated wires. The total slicing time was 11 hours, 41 minutes, giving an average cutting rate of 5.7 mils/min., 0.145 mm/min. This compares to 2.33 mils/min., 0.059 mm/min. obtained[2] with similar wires and 10 cm diameter workpiece before the present modification. This means that about 250% cutting rates have been achieved with increase in surface speed. These cutting rates are about 50% better than the projected cutting rates (0.1 mm/min.) in the

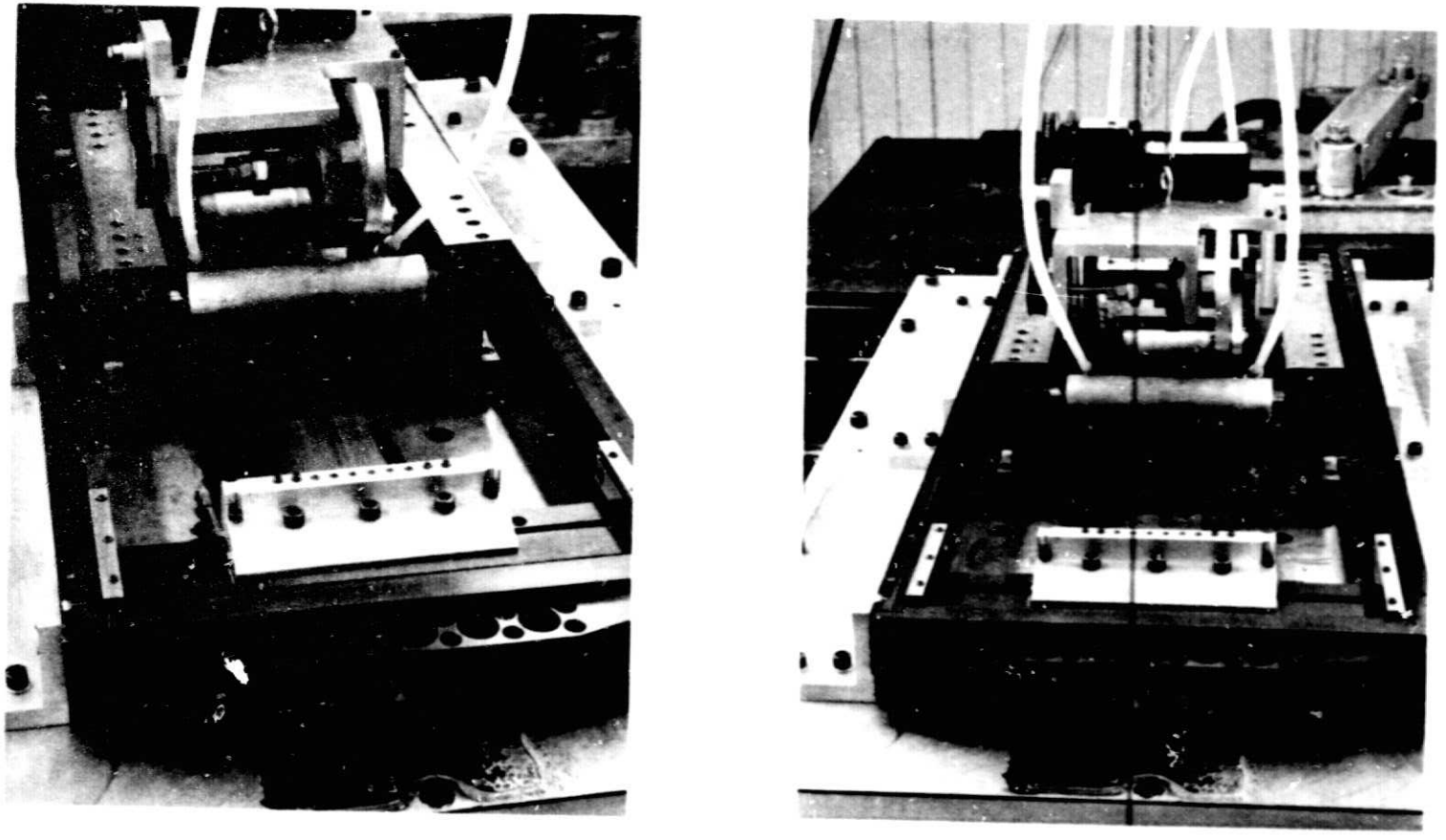

Figure 4. Two views of the high-speed slicer with light-weight bladehead

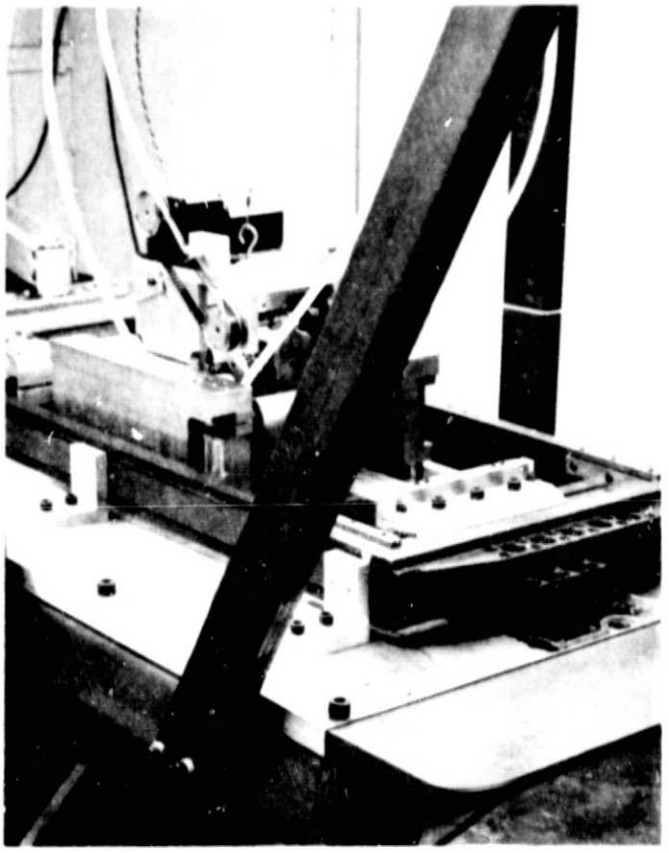

Figure 5. A view of the rocking mechanism incorporated in the high-speed slicer

TABLE II. SILICON SLICING SUMMARY

RUN	PURPOSE	FEED FORCE/BLADE lb	gm	AVERAGE CUTTING RATE mil/min	mm/min	WIRE TYPE	REMARKS
318-S	Life test continuation after dressing wires	0.070	31.9	2.38	0.060	5 mil, 0.125 mm W core electroplated with 30 μm diamonds	Higher cutting rates; 64% yield
319-S	Test plating from another source	N/A	N/A	N/A	N/A	Commercially impregnated wires electroless nickel plated, 0.3 mil, 7.5 μm	Run aborted due to poor cutting performance
320-S	Test modified plating	0.070	31.9	2.22	0.056	Commercially impregnated wire plated with a 0.3 mil, 7.5 μm nickel	Epoxy failure on mounting block. 50% yield.
321-S (15)	Life test	N/A	N/A	N/A	N/A	Same as 320-S	Run aborted due to diamond pull-out
322-S	Test 30 μm diamond electroplated wires	0.056	25.4	3.00	0.076	5 mil, 0.125 mm W core electroplated with 30 μm diamonds	Very good quality wafers; 100% yield
323-S	Life test	0.056	25.4	1.15	0.029	Same as 322-S	Good quality wafers; 92% yield
324-S	Life test continuation	0.056	25.4	1.04	0.026	Same as 322-S	Good quality wafers; 78% yield
325-SX	Slicing of 4" Ø ingot with high speed slicer	0.091	41.3	5.70	0.145	Commercially impregnated wire plated with 0.3 mil, 7.5 μm electroless nickel	Very high cutting rates. Roller degradation observed; 21% yield

(cont.)

TABLE II. SILICON SLICING SUMMARY (cont.)

RUN	PURPOSE	FEED FORCE/BLADE lb	gm	AVERAGE CUTTING RATE mil/min	mm/min	WIRE TYPE	REMARKS
326-S	Test impregnated wire	N/A	N/A	N/A	N/A	5 mil, 0.125 mm W core, 0.7 mil, 15.5 μm copper sheath impregnated with 30 μm diamonds; 7.5 μm electroless nickel	Run aborted as diamonds were buried.
327-SX	Test 30 m diamond electroplated wire	-	-	5.19	0.13	5 mil, 0.125 mm W core, electroplated with 30 μm diamonds	Non-uniformity in plating thickness on wire.

economic analysis for this technique.[3]

The yield obtained during run 325-SX was only 21%. It was found that during first half of the ingot, a 100% yield was maintained; however, from then on, breakage of wafers was observed. Examination after completion of the run showed that the guide rollers degraded; i.e., wires cut deep grooves into the rollers. The heavy mass of these rollers had too much inertia to change directions at such high speeds and the wire cut into them.

Similar high cutting rates were also achieved in run 327-SX even though the non-uniformity of the nickel plating on this bladepack is not conducive to effective slicing.

Blade Development

During this quarter it was found that very good cutting performance was achieved with 30 μm diamond electroplated wire--high yields and good wafer quality were obtained for four runs. In run 318-C these wires were used for a fifth run after dressing. It was found that the cutting rates achieved during this run were higher; however, only 64% yield was obtained. Visual examination showed absence of diamonds in some areas of the cutting edge. SEM examination of these wires revealed that swarf had dried up and formed a layer over the diamonds in some areas (Figure 6). These wires have given a good cutting performance and it has been maintained for five runs without much degradation. The cutting rates revived after dressing of wires.

Figure 6. Sections of wire showing swarf is covering the diamonds

A bladepack of commercially impregnated wire was plated with 7.5 μm nickel. During plating the solution was modified to see if the bond between the nickel and diamonds can be improved. These wires were used for slicing tests in run 320-S. Good cutting performance was achieved; however, during the second test (run 321-S) the wires stopped cutting towards the end of the run due to diamond pull-out.

Two significant developments have occurred in impregnation of diamonds into copper sheath. It has been found that it was possible to impregnate 45 μm size diamonds into 7.5 μm copper sheath. However, the copper was distorted. A 12.5 μm sheath was not distorted and the concentration of diamonds was very high. However, after plating the diamond concentration was not as high. Impregnation of 45 μm diamonds into 12.5 μm sheath was not deep enough and diamonds fell out during plating. Impregnation of 30 μm into a 15.5 μm copper sheath under high forces produced satisfactory impregnation and retention of diamonds. This showed that the diamonds have to be impregnated deep into the sheath with high pressure. However, as shown in run 326-S a 7.5 μm electroless nickel buries the diamonds.

So far the plated length of the wires has been equal to the stroke length of the slicer. It was found that at the end of the stroke a support roller and the workpiece passed over the transition area. Better performance was achieved when the diamond plated length was longer than the stroke length.

A similar bladepack used for runs 314-S through 318-S but with diamonds only in the cutting edge was used in runs 322-S through 324-S. Very effective slicing, good quality wafers, and 100% yield was achieved during the first run. Subsequently a deterioration in performance was observed. Examination of the bladepack after the third run showed that considerable diamond pull-out was observed.

A comparison of performance of this bladepack with a similar earlier one shows two significant differences which may explain the difference in their lives. Firstly, the present bladepack was electroplated on one side of the wire only. Secondly, the feed forces used in recent runs were lower, 25.7 gms. vs. 31.9 gms. used earlier. Both sets of wires were used at low surface speeds which is not conducive to effective slicing with fixed diamonds. These conditions put the diamond in a dragging mode. Further, it has been established[1] that higher feed forces result in enhanced cutting rates. Therefore, lower feed forces may be less conducive conditions for diamond slicing in addition to dragging mode at lower surface speeds.

CONCLUSIONS

1. Ingot casting has been extended to 16 cm x 16 cm square cross-section size. Ingots up to 8.1 kg have been cast.
2. Good crystallinity has been maintained for ingots using simpler power control.
3. A glass-working lathe makes it easier to achieve a uniform and reproducible graded structure in the crucibles.
4. Surface speeds of 500 feet per minute have been achieved with the 37 pound bladehead.
5. Higher forces used in impregnation helped retain diamonds during plating.
6. First slicing test on 10 cm diameter silicon after modifications have given average cutting rates of 5.7 mils/min., 0.145 mm/min. with impregnated wires.

REFERENCES

1. F. Schmid and C. P. Khattak, "Heat Exchanger--Ingot Casting/Slicing Process," ERDA/JPL 954373, Crystal Systems, Inc., Final Report (I), December 1, 1977.

2. F. Schmid and C. P. Khattak, "Heat Exchanger Method--Ingot Casting/Fixed Abrasive Method--Multi-Wire Slicing (Phase II)," DOE/JPL 954373, Crystal Systems, Inc., Monthly Progress Report No. 7, November 15, 1978.

3. F. Schmid and C. P. Khattak, "Heat Exchanger Method--Ingot Casting/Fixed Abrasive Method--Multi-Wire Slicing (Phase II)," DOE/JPL 954373, Crystal Systems, Inc., Quarterly Progress Report No. 3, July 15, 1978.

Contract 954173 (JPL)

MILESTONE CHART

Crystal Systems, Inc.

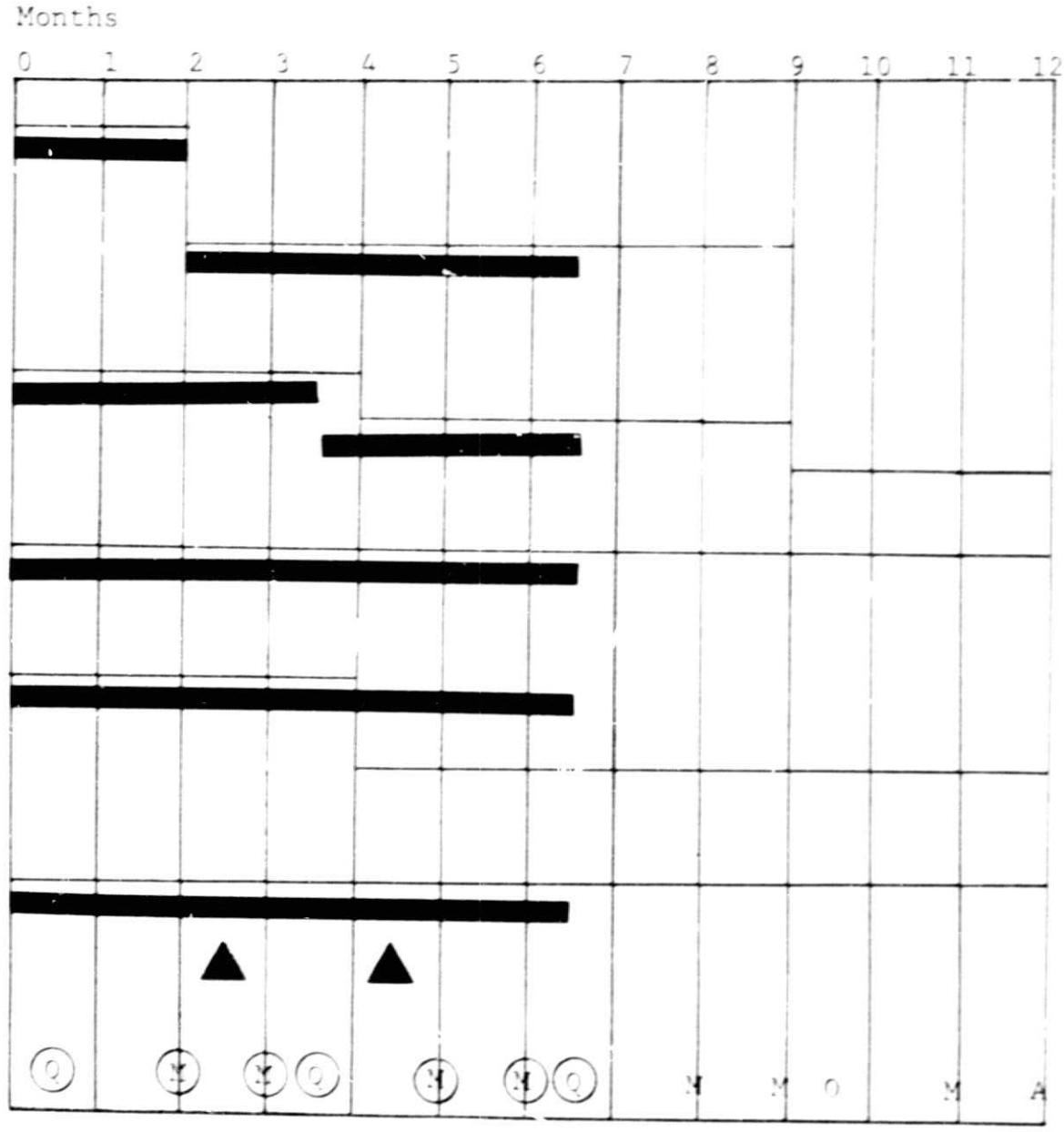

(*Modified milestone)

APPENDIX

Origin of SiC Impurities in Silicon Crystals Grown from the Melt in Vacuum

F. Schmid and C. P. Khattak
T. G. Digges, Jr.
Larry Kaufman

Journal of the
Electrochemical Society

Vol. 126, No. 6
June 1979

Origin of SiC Impurities in Silicon Crystals Grown from the Melt in Vacuum

F. Schmid* and C. P. Khattak

Crystal Systems Incorporated, Salem, Massachusetts 01970

T. G. Digges, Jr.[1]

Jet Propulsion Laboratory, Pasadena, California 91103

and Larry Kaufman

Manlabs, Incorporated, Cambridge, Massachusetts 02138

ABSTRACT

A main source of high carbon levels in silicon crystals grown from melt under reduced pressures and contained in silica crucibles supported by graphite retainer/susceptor has been identified by thermodynamic analysis. The calculations have been verified by experimental results and the carbon level can be reduced by approximately 50% with the use of molybdenum retainers.

The heat exchanger method (HEM) developed to grow large sapphire crystals (1-3) has been extended to the growth of silicon crystals (4). In this method the seed is placed at the bottom of the crucible and the temperature in the melt increases upwards. This suppresses convection that causes temperature and concentration fluctuations at the solid-liquid interface (5).

Early experiments indicated that SiC particles were found in crystals solidified by the HEM (6). However, even with the presence of SiC particles, large grains have been grown with limited interface breakdown during solidification. This observation was contradistinct to Czochralski (CZ) growth where interface breakdown due to SiC is followed by twin/polycrystalline growth (7).

The basic elements of the HEM and the CZ growth furnaces and the processes are quite similar (heaters, crucibles, insulation, etc.). A silica crucible loaded with the charge and set in a graphite retainer is placed in the furnace. The chamber is evacuated, and after melting the charge crystal growth is achieved. In the HEM process, the chamber is typically evacuated during growth to 0.1 Torr. For CZ growth an argon blanket is used and the chamber pressure can vary from 10 Torr to 1 atm (8). In early experiments with HEM growth it was quite surprising that high carbon concentrations were found in the silicon ingots. The purpose of this paper is to explain the origin of this carbon concentration and to present thermodynamic and experimental results that support the conclusions.

Reactions between Graphite and Silica

Silicon, oxygen, and carbon are used in the HEM in the form of silicon melt stock, silica crucibles and graphite furnace parts, and retainers. A thermodynamic evaluation has considered possible reactions between these three reactants and the salient reactions are reported.

Carbon has been observed in silicon crystals as silicon carbide. Silicon melt stock and graphite parts are not in direct contact; therefore, the following reactions between graphite and silica crucible were studied

$$2C + SiO_2 \rightarrow SiC + CO_2 \quad [1]$$

$$3C + 3SiO_2 \rightarrow SiC + 2CO_2 + 2SiO \quad [2]$$

$$4C + 2SiO_2 \rightarrow SiC + 3CO + SiO \quad [3]$$

$$3C + SiO_2 \rightarrow SiC + 2CO \quad [4]$$

In addition to the reactions forming SiC two additional reactions were considered

$$C + SiO_2 \rightarrow SiO + CO \quad [5]$$

$$C + 2SiO_2 \rightarrow 2SiO + CO_2 \quad [6]$$

Using the data in Table I, reactions [1]-[6] have positive free energy changes at atmospheric pressure and in the temperature range 1600°-1750°K (Table II) with those reactions that produce CO_2 tending to be more positive. The least positive free energies at atmospheric pressure are given by Eq. [4] and [5]. For reaction [5] the standard free energy of formation, $\Delta G°$, using data in Table I, is

$$\Delta G° = 162900 - 81T$$

Also

$$\Delta G = \Delta G° + RT \ln K$$

where R is the gas constant, T is temperature in degrees Kelvin, and K is the equilibrium constant for the reaction. Since equimolar ratios of SiO and CO are formed, their partial pressures are

$$p_{SiO} = p_{CO} = \tfrac{1}{2}\, p$$

where p is the total pressure. Under equilibrium conditions, $\Delta G = 0$, hence

$$\log p \text{ (atm)} = 9.15 - 1.78 \times 10^4/T$$

or

$$\log p \text{ (Torr)} = 12.03 - 1.78 \times 10^4/T$$

These equations are used to plot the curve (line) along with $\Delta G = 0$, i.e., C + SiO_2 is in equilibrium with SiO + CO. The line separates the range of T, p space in which C + SiO_2 has a lower free energy than

Table I. Standard free energy of formation, $\Delta G°$, in the temperature range 1300°-1800°K (Source: Manlabs-NPL Data Bank)

Compound*	$\Delta G°$ (cal/mol)
SiC (solid)	−18200 + 3T
CO (gas)	−28300 − 20T
CO_2 (gas)	−94700
SiO_2 (solid)	−218300 + 43T
SiO (gas)	−27100 − 18T

* Note: T = °K.

* Electrochemical Society Active Member.

[1] Present address: Virginia Semiconductor, Incorporated, Fredericksburg, Virginia 22401.

Key words: carbon, thermodynamics, transport, pressure.

Table II. Standard free energy change for various reactions as a function of temperature

	Reaction	ΔG (calories) 1600°K	1650°K	1700°K	1750°K
[1]	$2C + SiO_2 \rightarrow SiC + CO_2$	41,400	39,400	37,400	35,400
[2]	$3C + 3SiO_2 \rightarrow SiC + 2CO_2 + 2SiO$	133,000	125,800	117,700	109,600
[3]	$4C + 2SiO_2 \rightarrow SiC + 3CO + SiO$	48,800	40,750	32,700	24,650
[4]	$3C + SiO_2 \rightarrow SiC + 2CO$	15,500	11,500	7,500	3,500
[5]	$C + SiO_2 \rightarrow SiO + CO$	33,300	29,250	25,200	21,150
[6]	$C + 2SiO_2 \rightarrow 2SiO + CO_2$	92,500	86,400	80,300	74,200
[10]	$2C + SiO \rightarrow SiC + CO$	−17,800	−17,750	−17,700	−17,650
[11]	$3C + 2SiO \rightarrow 2SiC + CO_2$	−9,700	−7,600	−5,500	−3,400
[12]	$C + SiO \rightarrow Si + CO$	−4,400	−4,500	−4,600	−4,700

SiO + CO from a second range of T, p space where SiO + CO has a lower free energy than C + SiO_2. These ranges and the $\Delta G = 0$ equilibrium curve (line) are marked in Fig. 1. Similar data for Eq. [4], also plotted in Fig. 1, show that SiC may be formed by the reaction of carbon and silica, but do not explain how SiC is transported across the crucible wall into the silicon. This leads to the conclusion that SiC is formed by reaction of a gaseous reaction product.

It should be noted that in the HEM furnace the system pressure is measured about 6 in. outside the hot zone. Even though it may not represent the exact pressure in the hot zone, it is a good indication of the operating pressures in the hot zone.

Reactions Involving Reaction Products

In the above analysis it was found that the reaction between the materials in the HEM furnace did not explain the formation of silicon carbide. Further the reactions that produce CO_2 have a higher free energy than those involving CO. Examination of the reaction

$$C + CO_2 \rightarrow 2CO \qquad [7]$$

shows that it proceeds strongly to the right at 1700°K and pressures near 1 Torr (i.e., 10^{-3} atm). Thus CO will be the dominant reactant. This conclusion would be further emphasized if graphite were to react with oxygen in place of CO_2 in Eq. [7].

Another vapor species expected in the HEM furnace is SiO. This is formed by the reaction of molten silicon with the silica crucible (9, 10)

$$Si + SiO_2 \rightarrow 2SiO \qquad [8]$$

The equilibrium vapor pressure of gaseous SiO as a function of temperature for this reaction is plotted in Fig. 2.

The reaction involving the two dominant vapor species, CO and SiO, has been examined

$$CO + 3SiO \rightarrow SiC + 2SiO_2 \qquad [9]$$

and the results plotted as a function of pressure and temperature in Fig. 3. It can be seen that under the operating experimental conditions, this reaction does not proceed to the right.

Examination of the following reactions between graphite and SiO show that in two cases SiC is formed

$$2C + SiO \rightarrow SiC + CO \qquad [10]$$

$$3C + 2SiO \rightarrow 2SiC + CO_2 \qquad [11]$$

$$C + SiO \rightarrow Si + CO \qquad [12]$$

The free energy of these reactions at atmospheric

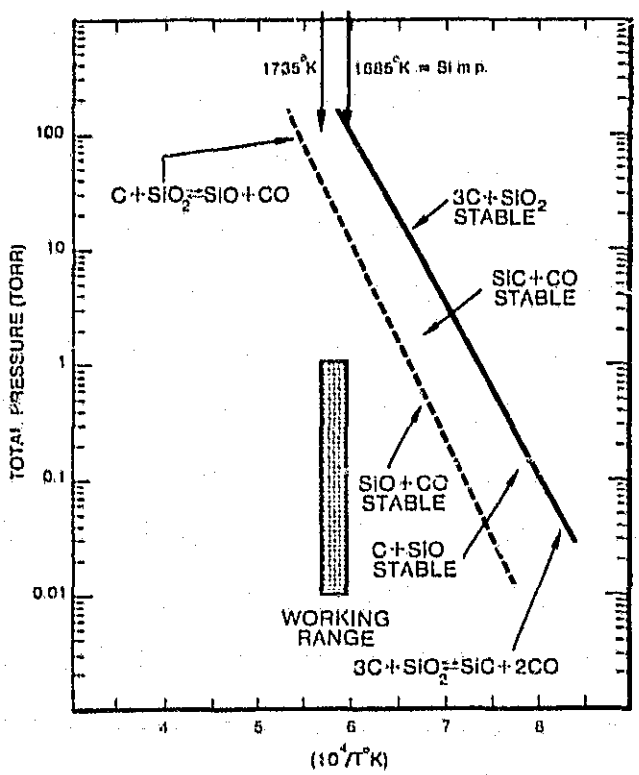

Fig. 1. Calculated pressure-temperature relations for reaction of graphite and silica to form silicon carbide, silicon monoxide, and carbon monoxide.

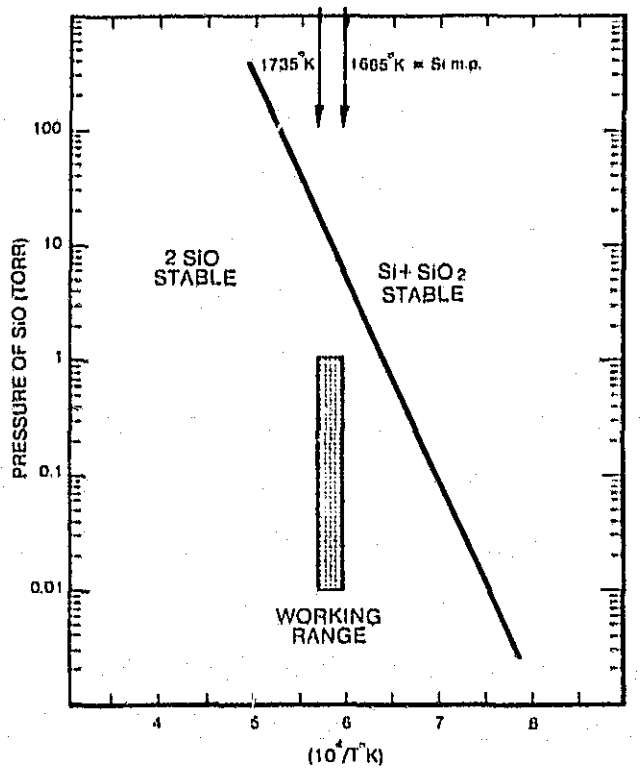

Fig. 2. Equilibrium vapor pressure of gaseous SiO as a function of temperature for the reaction Si (condensed) + SiO_2 (condensed) → 2SiO (gas).

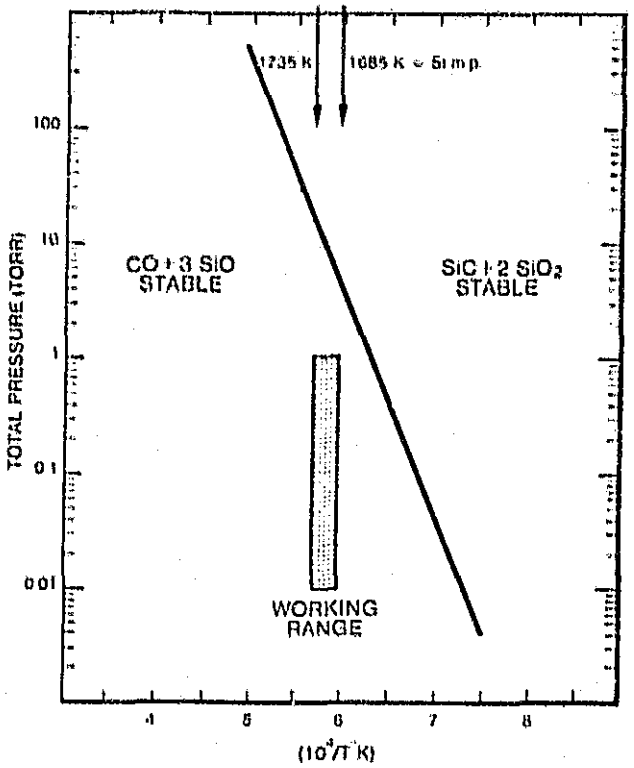

Fig. 3. Equilibrium total pressure of CO and SiO as a function of temperature for the reaction $CO + 3SiO \rightarrow SiC + 2SiO_2$.

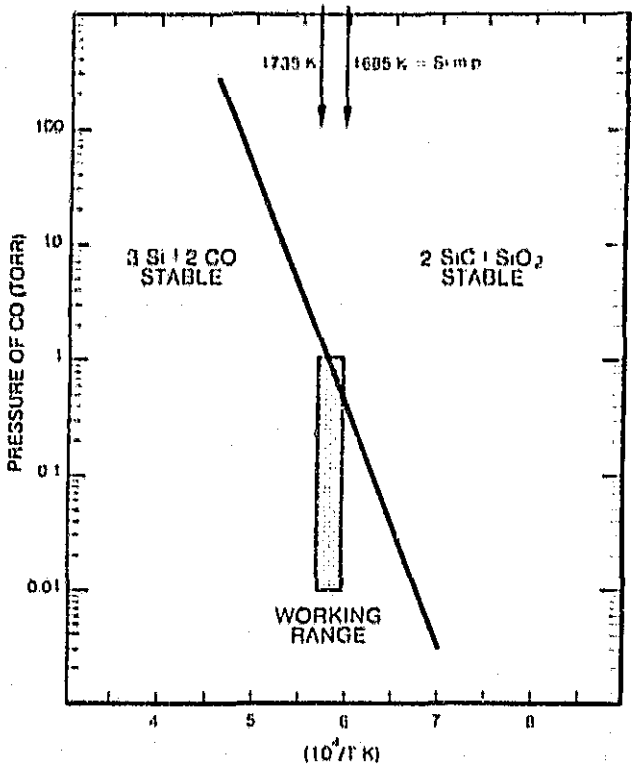

Fig. 4. Equilibrium pressure of CO as a function of temperature for the reaction $2CO + 3Si \rightarrow 2SiC + SiO_2$.

pressure is negative (Table II). This will result in coating of the furnace parts with SiC, yet no contamination of the silicon.

The following reactions involving CO and Si were studied

$$Si + CO \rightarrow SiC + \tfrac{1}{2} O_2 \quad [13]$$

$$3Si + 2CO \rightarrow 2SiC + SiO_2 \quad [14]$$

$$2Si + CO \rightarrow SiC + SiO \quad [15]$$

Reaction [13] yields a positive free energy at atmospheric pressure. Considering the pressure and temperature dependence of this reaction, the reactants will be stable in the experimental operating conditions (10). The stability range of reaction [14] shows that the reactants are stable (Fig. 4). The standard free energy of reaction [15], $\Delta G°$, using data in Table I can be represented by Eq [16] where T = °K

$$\Delta G° = -17{,}000 + 5T \text{ (calories)} \quad [16]$$

This reaction proceeds to the right at 1700°K. The free energy of the reaction, ΔG, utilizing the usual free energy relationship, can be calculated from

$$\Delta G = \Delta G° + RT \ln K \quad [17]$$

Assuming unit activity in the condensed phase and p_{SiO}, p_{CO} (the partial pressures of SiO and CO respectively), Eq. [17] can be written as

$$\Delta G = -17{,}000 + 5T + 1.987T \ln (p_{SiO}/p_{CO}) \quad [18]$$

If the equilibrium fraction of SiO can be represented by x, then

$$x = \exp\left(\frac{17{,}000 - 5T}{1.987T}\right) \Big/ \left[1 + \exp\left\{\left(\frac{17{,}000 - 5T}{1.987T}\right)\right\}\right] \quad [19]$$

The corresponding fractions of the vapor species at different temperatures are shown in Table III. Therefore, a major source of silicon carbide formation in silicon can come from reaction [15]. The vapor pressure of carbon over graphite is less than 10^{-11} Torr at the melting point of silicon and can, therefore, be ignored. The formation of CO, besides a vacuum leak and reaction of absorbed gases on graphite parts, is from reactions [4] and [5]. This appears to be the most likely source for transport of C to the silicon.

Reactions [1]-[15] and Table I cover 9 of the 12 reactions cited by Coldwell (11). The three remaining reactions discussed in Coldwell's paper and ignored here deal with the reduction of SiO_2 and/or SiO by carbon to form silicon. These reactions are unlikely in the T, p range under consideration here. The present analysis is concerned with a wide range of pressure in contrast to Coldwell's discussion which is confined to 1 atm conditions.

Experimental Verification

The above thermodynamic analysis indicates that SiC in HEM grown silicon is attributable to the reaction of CO and Si. A major source of CO is from reactions [4] and [5], interaction of silica crucible with graphite retainer. This was verified indirectly by experiment. A graphite piece was sandwiched between two pieces of single crystal silicon with polycrystalline silicon around them. The furnace was heated close to the melting point of silicon and cooled. It was found that a silicon carbide layer was formed in areas where the graphite was in contact with the silicon crystals and also a light layer was found in the immediate vicinity. The pieces far removed from the graphite piece

Table III. Equilibrium fraction of CO and SiO at various temperatures in reaction [15]

T (°K)	$x = p_{SiO}/P_t$	% CO	% SiO
1650	0.935	6.5	93.5
1687	0.928	7.2	92.8
1700	0.925	7.5	92.5
1750	0.915	8.5	91.5

$P_t = p_{SiO} + p_{CO}$.

showed no evidence of SiC. In this experiment the graphite piece was not in contact with silica, hence reactions [4] and [5] were suppressed. In another run when the charge was heated in a silica crucible held in a graphite retainer and cooled, the entire melt stock was coated with SiC.

Experimental evidence of SiC formed in HEM grown silicon is shown in Fig. 5 and 6. Silicon carbide has accumulated at the solid liquid interface. The sample has been etched with CP-4. The groove represents a boundary where spontaneous nucleation and freezing from the top of the liquid has met the advancing interface solidifying from the bottom towards the top. In this growth a graphite retainer was used and the operating pressure was 0.1 Torr. The precipitates were identified by x-ray dispersive analysis. Infrared measurements indicated a concentration of carbon in the (3.5-4.1) $\times$ 10^{17} atoms/cm^3 range which is close to the solid solubility limit near the melting point of silicon (12). The entire top surface of the solidified ingot was covered with SiC. A similar experiment carried out with a molybdenum retainer indicated a carbon concentration of (1.5-3.1) $\times$ 10^{17} atoms/cm^3 for twelve samples. The top surface of the ingot was clean and shiny with no evidence of the SiC layers. The replacement of graphite retainer with molybdenum resulted in lower carbon levels in silicon. This eliminated the contact of graphite with the silica crucible. As far as reactions involving O_2, H_2 and water absorption in graphite, they will not be changed significantly because the HEM is carried out in a resistance heated furnace which has all graphite parts (*e.g.*, heater, liner, insulation, etc.).

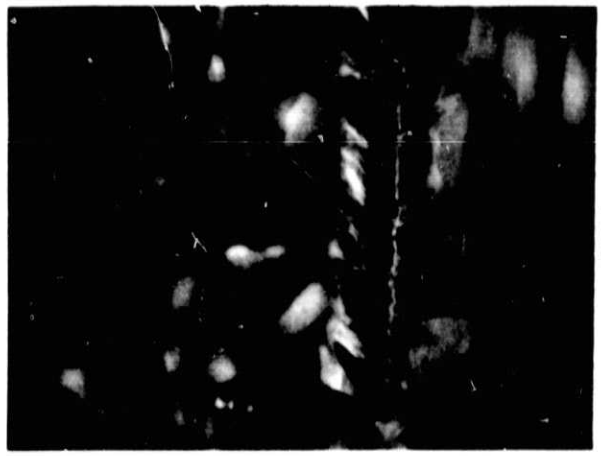

Fig. 5. Optical photograph (320×) showing the freeze line described in text.

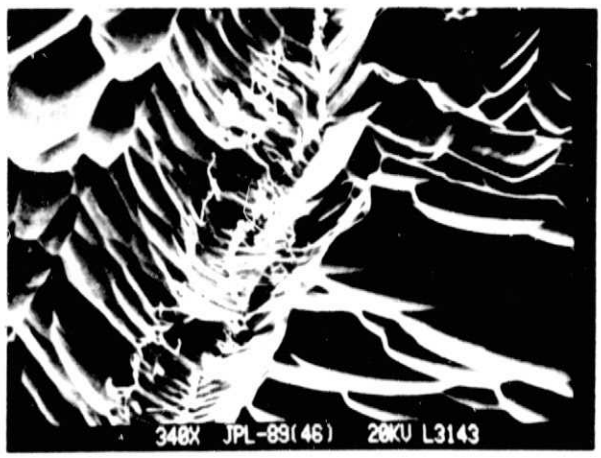

Fig. 6. SEM photograph (340×) illustrates details of dendrite growth. Energy dispersive analysis of a single dendrite showed it to be SiC.

Conclusions

Evidence of high carbon levels in HEM grown silicon have led to a proposed mechanism for the cause of silicon carbide formation. It is associated with the use of graphite retainers in contact with silica crucibles under reduced pressures. High carbon levels in silicon have been reported to cause breakdown in crystallinity in CZ (7, 13) as well as in ribbon growth (14). The electrical effects of SiC inclusions have been detrimental in solar cell devices (15). The origin of high carbon levels in silicon processed in vacuum is because of reactions between silica crucibles and graphite retainers. If the graphite retainers are replaced by molybdenum, these reactions do not take place, and thereby the carbon levels in the silicon can be considerably reduced.

Acknowledgment

This paper presents results of research performed for the Low-Cost Solar Array Project, Jet Propulsion Laboratory, California Institute of Technology, sponsored by the U.S. Department of Energy through an interagency agreement with the National Aeronautics and Space Administration.

Manuscript submitted June 22, 1978; revised manuscript received Sept. 6, 1978.

Any discussion of this paper will appear in a Discussion Section to be published in the December 1979 JOURNAL. All discussions for the December 1979 Discussion Section should be submitted by Aug. 1, 1979.

Publication costs of this article were assisted by Crystal Systems Incorporated.

REFERENCES

1. F. Schmid and D. Viechnicki, *J. Am. Ceram. Soc.*, **53**, 528 (1970).
2. F. Schmid and D. Viechnicki, *Solid State Technol.*, **16**, 45 (1973).
3. D. Viechnicki and F. Schmid, *J. Cryst. Growth*, **26**, 162 (1974).
4. C. P. Khattak and F. Schmid, *Am. Ceram. Soc. Bull.*, **57**, 609 (1978).
5. K. M. Kim, A. F. Witt, and H. C. Gatos, *J. Mater. Sci.*, **6**, 1036 (1971).
6. T. G. Digges, Jr., M. H. Liepold, K. M. Koliwad, G. Turner, and G. D. Cumming, 12th IEEE Photovoltaic Specialists Conference, Baton Rouge, La. (1976).
7. F. W. Voltmer and F. A. Padovani, in "Semiconductor Silicon 1973," H. R. Huff and R. R. Burgess, Editors, p. 75, The Electrochemical Society Softbound Symposium Series, Princeton, N.J. (1973).
8. C. P. Chartier and C. B. Sibley, *Solid State Technol.*, **18**, 42 (1975).
9. H. D. Erasmus and J. A. Persson, *Trans. Electrochem. Soc.*, **95**, 316 (1949).
10. F. Schmid and C. P. Khattak, ERDA/JPL 954373, 8th Quarterly Progress Report, October 1977.
11. D. M. Coldwell, *High Temp. Sci.*, **8**, 309 (1976).
12. R. G. Newman and J. Wakefield, "Metallurgy of Semiconductor Materials," Interscience Publ., New York (1962).
13. S. N. Rea and P. S. Gleim, ERDA/JPL 954475, Final Report, p. 29, April 1977.
14. T. F. Ciszek, *Mater. Res. Bull.*, **7**, 731 (1972).
15. C. V. Hari Rao, H. E. Bates, and K. V. Ravi, *J. Appl. Phys.*, **47**, 2614 (1976).